Electrically Silent Divalent Cation Entries in Resting and Active Voltage-Controlled Muscle Fibers

Céline Berbey and Bruno Allard*
Physiologie Intégrative Cellulaire et Moléculaire, Université Lyon 1, Centre National de la Recherche Scientifique Unité Mixte de Recherche 5123, Villeurbanne, France

ABSTRACT Ca^{2+} is known to enter skeletal muscle at rest and during activity. Except for the well-characterized Ca^{2+} entry through L-type channels, pathways involved in these Ca^{2+} entries remain elusive in adult muscle. This study investigates Ca^{2+} influx at rest and during activity using the method of Mn^{2+} quenching of fura-2 fluorescence on voltage-controlled adult skeletal muscle cells. Resting rate of Mn^{2+} influx depended on external [Mn^{2+}] and membrane potential. At −80 mV, replacement of Mg^{2+} by Mn^{2+} gave rise to an outward current associated with an increase in cell input resistance. Calibration of fura-2 response indicated that Mn^{2+} influx was too small to be resolved as a macroscopic current. Partial depletion of the sarcoplasmic reticulum induced by a train of action potentials in the presence of cyclopiazonic acid led to a slight increase in resting Mn^{2+} influx but no change in cell input resistance and membrane potential. Trains of action potentials considerably increased Mn^{2+} entry through an electrically silent pathway independent of L-type channels, which provided 24% of the global Mn^{2+} influx at +30 mV under voltage-clamp conditions. Within this context, the nature and the physiological role of the Ca^{2+} pathways involved during muscle excitation still remain open questions.

INTRODUCTION

In skeletal muscle, Ca^{2+} ions triggering contraction are released from the sarcoplasmic reticulum (SR) in response to depolarization of the cell. In parallel to these massive variations of intracellular Ca^{2+}, a Ca^{2+} influx is also known to occur through the sarcolemma in both resting and working muscle.

Early measurements using radiolabeled Ca^{2+} have shown that Ca^{2+} slowly enters skeletal muscle cells in resting conditions (1). The physiological role of this Ca^{2+} entry is poorly understood in normal muscle but several lines of evidence suggest that a chronic elevation of the resting influx of Ca^{2+} might contribute to the initiation or progression of muscle cell degeneration in a number of muscle disorders (2). Within this context of potential pathophysiological consequences of exacerbated Ca^{2+} entry, the study of resting Ca^{2+} influx and the search for the pathways through which it takes place are of fundamental interest. A widespread hypothesis suggests that Ca^{2+} enters resting muscle cell through ion channels. Single channel recordings indeed revealed opening of poorly selective cation channels carrying inward current at negative membrane potentials in isolated mouse skeletal muscle fibers (3–6). However, subsarcolemmal Ca^{2+} load revealed by the measurement of Ca^{2+}-activated K^+ channel opening was found to be independent of the activity of the spontaneously active Ca^{2+} channels, suggesting the existence of electrically silent sites of passive Ca^{2+} influx (7). Additionally, certainly because of the absence of specific inhibitors of resting Ca^{2+} influx and because of the drastic modifications of the electrophysiological muscle properties resulting from manipulation of external Ca^{2+}, there is no experimental evidence available demonstrating the development of a Ca^{2+} current at the whole cell level under resting conditions.

Another way to monitor Ca^{2+} influx at rest is to measure the changes in fluorescence of Ca^{2+} dyes. Early works investigating plasmalemmal divalent cations influx in nonexcitable cells have introduced the use of Mn^{2+} as a surrogate of Ca^{2+} to directly assess Ca^{2+} entry (e.g., 8). Mn^{2+} ions are assumed to penetrate cells through the same pathways as the ones used by Ca^{2+}, and, once within the cells, these ions are trapped in the cytosol and strongly quench the fluorescence emitted by Ca^{2+} dyes. In adult skeletal muscle, this Mn^{2+}-quenching method has been used to confirm that the muscle sarcolemma has a substantial permeability to divalent cations under resting conditions, but they were performed in the absence of voltage control and therefore did not establish whether Mn^{2+} entry generated a measurable macroscopic membrane current whose properties could give evidence for the existence of ion channels open at rest, permeable to Mn^{2+} and Ca^{2+} (e.g., 9). The Mn^{2+}-quenching method has also been used to show that SR depletion induced in the presence of SR Ca^{2+}-ATPase inhibitors gave rise to an increase in resting Ca^{2+} influx in adult and fetal muscle fibers (10,11). However, using voltage clamp on adult muscle fibers, Allard et al. (12) demonstrated that SR depletion was not associated with the generation of a resting inward current thus challenging the physiological relevance of a store-operated membrane conductance in adult skeletal muscle.

In working adult muscle, depolarization elicits a well-characterized Ca^{2+} entry through L-type Ca^{2+} channels early recorded as a voltage-activated current. But more recently, using the Mn^{2+}-quenching method in primary

Submitted October 28, 2008, and accepted for publication January 6, 2009.

*Correspondence: bruno.allard@univ-lyon1.fr

Editor: David A. Eisner.

0006-3495/09/04/2648/10 $2.00

doi: 10.1016/j.bpj.2009.01.008

myotubes, Cherednichenko et al. (13) demonstrated that membrane depolarization initiated a Ca^{2+} entry independent of the voltage-gated L-type Ca^{2+} current and of SR depletion. An increased Ca^{2+} entry provoked by KCl depolarization was also recently described in adult muscle (14), but there was no attempt to determine if this Ca^{2+} entry was independent of the voltage-activated L-type Ca^{2+} current as found in myotubes. There is also no available information about the behavior of this Ca^{2+} influx as a function of the membrane voltage, although membrane voltage is recognized to tightly control Ca^{2+} changes in skeletal muscle.

This study is the first, to our knowledge, to combine the Mn^{2+}-quenching method and voltage control on adult mouse skeletal muscle cell to investigate sarcolemmal Ca^{2+} influx under resting and active conditions. Monitoring of the background membrane current during Mn^{2+} influx together with calibration of the fura-2 response to Mn^{2+} led us to conclude that the Mn^{2+} influx at rest and in response to partial depletion of the SR does not induce any resolvable macroscopic current. We also demonstrate that the rate of Mn^{2+} entry is markedly increased by tetanic muscle activity principally through an electrically silent voltage-dependent Ca^{2+} entry independent of the voltage activated L-type current.

MATERIALS AND METHODS

Preparation of muscle fibers

Experiments were performed on single skeletal fibers enzymatically isolated from interosseal muscles of adult male Swiss OF1 mice. All experiments were performed in accordance with the guidelines of the French Ministry of Agriculture (87/848) and of the European Community (86/609/EEC). Procedures for enzymatic isolation of single muscle fibers and partial insulation of the fibers with silicone grease were as described previously (15). In brief, the major part of a single fiber (between 0.5 and 1 mm length) was electrically insulated with silicone grease so that a fiber portion between 50 and 100 μm length was let free of grease. A micropipette was then inserted into the fiber through the silicone layer. Under these conditions, whole-cell voltage clamp could be achieved on the portion of the fiber extremity free of grease. The tip of the micropipette was then crushed into the dish bottom to allow intracellular dialysis of the fiber (16).

Electrophysiology

Fibers were voltage clamped with an RK-400 patch-clamp amplifier (Bio-Logic, Claix, France) used in the whole-cell configuration. Command voltage pulse generation and data acquisition were done using the pClamp10 software (Axon Instruments Inc., Downington, PA) driving an A/D converter (Digidata 1322A, Axon Instruments Inc.). Analog compensation was systematically used to decrease the effective series resistance. Voltage clamp was performed with a microelectrode filled with the whole-cell intrapipette solution (see Solutions). Cell capacitance was determined by integration of a current trace obtained with a 10-mV hyperpolarizing pulse from the holding potential and used to calculate the density of Mn^{2+} currents (A/F). For voltage activated currents, leak currents were subtracted from all recordings using a 10-mV hyperpolarizing pulse preceding every test pulse from the holding potential supposing a linear evolution of leak current with depolarization. The voltage dependence of the mean Mn^{2+} current density was fitted using the following equation: $I(V) = G_{max}\ (V - V_{rev})/((1 + \exp((V_{0.5} - V)/k)))$, where $I(V)$ is the mean density of the current measured, V the test pulse, G_{max} the maximum conductance, V_{rev} the apparent reversal potential, $V_{0.5}$ the half-activation voltage, and k a steepness factor. The voltage dependence of the normalized conductance was obtained by dividing $I(V)$ by $G_{max}\ (V - V_{rev})$.

Mn^{2+}-quenching experiments

Before experiments, cells were dialyzed for 20 min with an internal pipette solution containing 100 μM fura-2 (see earlier discussion) and imaged with an inverted microscope (Nikon Diaphot) equipped for epifluorescence using a 40× oil-immersion objective. Fura-2 fluorescence was measured with monochromatic excitation at a Ca^{2+}-insensitive wavelength (360 nm) (T.I.L.L. Photonics, Martinsried, Germany). Images from a circular region of 20 μm diameter centered on the silicone-free extremity of the cell under study were captured with a Darkstar 800 device camera (Photonic Science, Robertsbridge, UK) at a frequency of 0.2 Hz or 0.1 Hz. This low sampling rate was chosen so that cells were exposed to the excitation beam for a very short time (200 ms) during image capture to make photo-bleaching negligible. Image acquisition and processing were performed using the Axon Imaging Workbench (Axon Instruments Inc.). Fluorescence values were expressed as percentage of the initial fluorescence recorded before addition of Mn^{2+} to the external medium, corrected for background fluorescence. Under resting conditions, the rate of fluorescence quenching was determined by fitting a linear regression to the fluorescence records. In response to a train of action potentials (AP) or to voltage pulses, given the low image acquisition frequency, the Mn^{2+} influx rate was extrapolated from the absolute decrease in fluorescence between two fluorescence data points.

In vitro and in vivo calibration of Mn^{2+} quenching

For in vitro calibration, the fura-2 fluorescence was measured on pulled glass tubes of 50 μm internal diameter filled with an aqueous solution containing 100 μM fura-2 and various [$MnCl_2$]. For in vivo calibration, cells dialyzed with an internal solution containing 100 μM fura-2 were exposed to a solution containing (in mM) 140 K-glutamate, 10 HEPES adjusted to pH 7.2 with K-OH, and 20 μM ionomycin. Increasing concentrations of $MnCl_2$ were added in this external solution, and the fura-2 fluorescence was measured after fluorescence intensity had reached a new steady state.

Estimation of Mn^{2+} current intensity on the basis of Mn^{2+}-quenching rates

The membrane surface area was estimated by measuring the capacitance of the portion of the cell under study and assuming a specific capacitance of 4.5 μF/cm^2 (17). This surface value was used to estimate the cell volume into which Mn^{2+} diluted once within the cell assuming an average cell diameter of 40 μm. The quenching rate (%/min) recorded in every cell was then converted into intracellular Mn^{2+} concentration reached after 1 min using the relationship obtained between the relative fluorescence intensity emitted by the fibers and the external concentration of Mn^{2+} in the presence of ionomycin (see above and Fig. 4). This intracellular concentration allowed us to estimate the quantity of divalent charges accumulated in the calculated cell volume after 1 min which in turn, divided by 60 and by the value of cell capacitance, yielded the density of Mn^{2+} current that should have flowed through the sarcolemma.

Solutions

For experiments described in with Figs. 1, 5, *B* and *C*, and 7 *C*, the external saline corresponded to a standard Tyrode solution containing (in mM) 140 NaCl, 5 KCl, and 10 HEPES adjusted to pH 7.2 with NaOH with no added Ca^{2+} and various concentrations of $MgCl_2$. $MgCl_2$ was replaced by $MnCl_2$ at equimolar concentrations to minimize surface charge effects. For experiments described in Fig. 5 *A*, 1 mM $MnCl_2$ was added in a Tyrode solution containing 2 mM $CaCl_2$ and 2 mM $MgCl_2$. For experiments described in Figs. 2, 3, 6, and 7, *A*, *B*, and *D*, the external solution contained (in mM) 140 tetraethylammonium (TEA)-methanesulfonate, 10 HEPES

adjusted to pH 7.2 with TEA-OH with no added Ca^{2+}, and various concentrations of $MgCl_2$. $MgCl_2$ was replaced by $MnCl_2$ at equimolar concentrations. For experiments described in Figs. 6 and 7 *A*, 1.5 mM 4-aminopyridine was added in the external solution. The whole-cell intrapipette solution contained (in mM) 120 K-glutamate, 5 Na_2-ATP, 5 Na_2-phosphocreatine, 5.5 $MgCl_2$, 5 glucose, 5 HEPES adjusted to pH 7.2 with K-OH except for experiments described in Fig. 3 where the intrapipette solution contained (in mM) 120 Cs-aspartate, 5 Na_2-ATP, 5.5 $MgCl_2$, 5 glucose, 0.1 EGTA, 5 HEPES adjusted to pH 7.2 with Cs-OH. Fura-2 was dissolved in water at 10 mM, and cyclopiazonic acid (CPA), 9-anthracene carboxylic acid (9AC), and ionomycin were dissolved in dimethylsulfoxide at 50 mM, 100 mM, and 1 mM, respectively, and diluted to the required concentration in the solutions. Cells were exposed to different solutions by placing them in the mouth of a perfusion tube from which flowed by gravity the rapidly exchanged solutions. Experiments were carried out at room temperature.

Statistics

Least-squares fits were performed using a Marquardt-Levenberg algorithm routine included in Microcal Origin (Microcal Software Inc., Northampton, MA). Data are given as mean ± SE and compared using unpaired or paired *t*-tests or ANOVA as indicated in the text. Differences were considered significant when $p < 0.05$.

RESULTS

Divalent cation influx at rest

Fig. 1 illustrates the quenching of fura-2 fluorescence in fibers voltage clamped at −80 mV in response to the addition of various concentrations of Mn^{2+} in Ca^{2+}-free external solutions. Replacement of 3 mM Mg^{2+} by 3 mM Mn^{2+} in the external solution induced a marked reduction of the fura-2 fluorescence, which remained at a stabilized lower value upon removal of Mn^{2+} (Fig. 1 *A*). As long as the fluorescence signal remained higher than 50% of its initial value, it declined linearly with time so that the rate of quenching could be estimated by fitting the fluorescence decline with a linear regression. Fig. 1 *B* shows that the rate of fluorescence decline was dependent on the external [Mn^{2+}]. On average, an elevation of the external concentration of Mn^{2+} induced a significant gradual increase in the rate of quenching (Fig. 1 *C*) ($p = 0.0075$, ANOVA). When 2 mM Ca^{2+} was added to a 10 mM Mn^{2+}-containing Tyrode solution, the rate of quenching was approximately reduced by half ($p = 0.02$, unpaired *t*-test).

A second set of experiments was performed to determine how the rate of quenching was affected by the membrane potential. To improve the control of the membrane potential, cells were bathed in an external solution containing 140 mM TEA-methanesulfonate. Fig. 2 *A* presents the drop of fluorescence induced by replacement of 3 mM external Mg^{2+} by Mn^{2+} in four different cells held at +40, 0, −40, or −80 mV. On average, Fig. 2 *B* shows that the less negative the membrane potential, the lower the rate of quenching ($p = 0.019$, ANOVA). The effect of a change in membrane potential on the rate of Mn^{2+} quenching could also be revealed on a same fiber. A hyperpolarization of 60 mV amplitude indeed induced

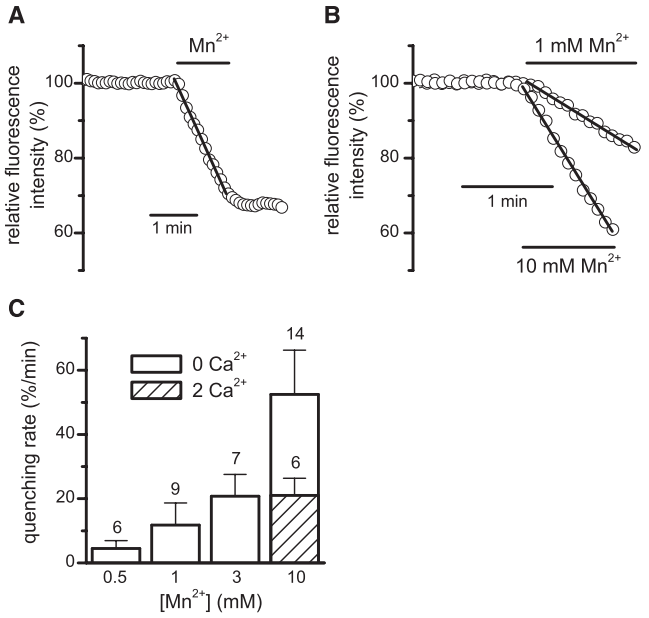

FIGURE 1 Influence of the external Mn^{2+} concentration on Mn^{2+} influx at −80 mV. The bars indicate the periods during which the cell was exposed to an external Tyrode solution containing 3 mM Mn^{2+} (*A*) and 1 mM or 10 mM Mn^{2+} (*B*). The straight lines superimposed correspond to the linear regressions fitted to the fluorescence records with slopes of 27%/min in (*A*) and 14 and 38%/min in (*B*). (*C*) The histogram shows the average values of quenching rate obtained in the presence of increasing external Mn^{2+} concentrations. The numbers above each bar indicate the number of cells tested.

an increase of the rate of quenching but depended on the initial value of the holding potential (Fig. 2 *C*). Fig. 2 *D* clearly illustrates that, on average, the more depolarized the initial holding potential, the lower the factor of increase of the quenching rate induced by the 60-mV negative voltage step.

Membrane current associated with resting cation influx

We next tried to determine if the influx of Mn^{2+} ion responsible for the quenching of fura-2 fluorescence was associated with a measurable macroscopic inward current. Fig. 3 shows that, at a holding potential of −80 mV, replacement of 3 mM Mg^{2+} by Mn^{2+} led to the development of an outward current associated with the quenching of fluorescence. In another cell held at +40 mV, the same maneuver gave rise to an inward current associated with a lower rate of quenching of fluorescence (Fig. 3 *B*). The same respective behaviors were observed in 10 fibers tested at −80 mV and in 7 fibers tested at +40 mV. To determine whether the outward current that developed at −80 mV in response to replacement of Mg^{2+} by Mn^{2+} resulted from the opening or closing of ion channels, the input resistance was challenged by applying every 5 s voltage ramps bringing the holding potential from −40 to −100 mV. To minimize the contribution of Cl^- and K^+ channels, cells were dialyzed with a Cs-aspartate–containing solution and the Cl^- blocker 9AC was added

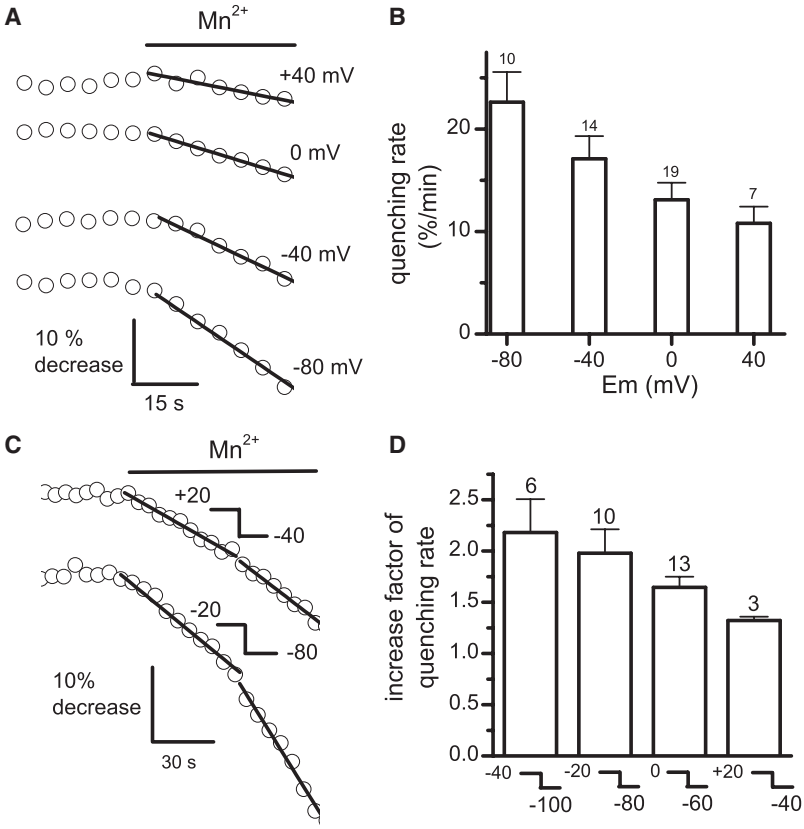

FIGURE 2 Influence of membrane potential on Mn^{2+} influx in the presence of 3 mM external Mn^{2+}. (*A*) Effect of addition of Mn^{2+} on fura-2 fluorescence at the indicated voltages in four different cells. The slopes of the linear fits are 8%, 13%, 20%, and 29%/min at +40, 0, −40, and −80 mV, respectively. (*B*) Average values of quenching rate obtained at different membrane voltages. (*C*) Changes in the quenching rate induced by a 60mV-hyperpolarizing pulse given from a holding potential of +20 mV (*upper trace*) and −20 mV (*lower trace*). The slope of the linear fits increased from 9% to 13%/min in the upper trace and from 15% to 29%/min in the lower trace. (*D*) Effect of the holding potential on the change in the quenching rate induced by a 60mV-hyperpolarizing pulse.

in the TEA-methanesulfonate–containing external solution. Also, 10 mM Mg^{2+} was replaced by 10 mM Mn^{2+} to strengthen the inwardly directed Mn^{2+} concentration gradient. Figs. 3, *C* and *D* show that replacement of Mg^{2+} by Mn^{2+} gave rise to a robust and reversible outward current associated with a decrease in the cell electrical conductance as evidenced by the decrease in the slope of the current induced by the voltage ramp. In 8 cells tested, the density of the inward background current at −80 mV was reduced from 3.13 ± 0.32 to 2.65 ± 0.26 A/F, whereas the cell conductance was reduced from 50 ± 5 to 43 ± 4 S/F upon replacement of Mg^{2+} by Mn^{2+}, both of which represents a 14.6 ± 1.8% decrease ($p < 0.001$, paired *t*-test). This result indicates that the main effect of external Mn^{2+} is to block spontaneously active ion channels carrying inward currents at −80 mV rather than to open channels carrying outward currents. It has to be mentioned that lower Mn^{2+} concentrations (1 mM or 100 μM), which, as expected, induced a weaker blocking effect but concomitantly reduced the Mn^{2+} concentration gradient, never elicited any discernable inward current at negative membrane potentials (unpublished). The nature of the ion channels blocked by Mn^{2+} was not further investigated.

Another possible interpretation of these results is that the inward current generated by the Mn^{2+} entry is too minute to be resolved under voltage-clamp conditions and may be masked by a predominant blocking effect of Mn^{2+} on resting conductances. To address this question, we measured the in vitro and in vivo potency of Mn^{2+} to extinguish the fura-2 fluorescence (see Methods) so that the intracellular [Mn^{2+}] that should be reached and, consequently, the Mn^{2+} current that should flow through the sarcolemma could be estimated. The Mn^{2+}-induced quenching of fura-2 fluorescence obtained in glass tubes is shown in Fig. 4 *A* (*open symbols*). Fitting the relationship between the mean relative change in fura-2 fluorescence and the [Mn^{2+}] with a Hill equation gave values of $K_{0.5}$ and N of 24 μM and 1. The Mn^{2+}-induced quenching of fura-2 fluorescence was also measured in vivo by exposing fibers to various [Mn^{2+}] in the presence of the Ca^{2+} ionophore ionomycin (Fig. 4 *B*). Fitting the relationship between the mean relative change in fura-2 fluorescence and the [Mn^{2+}] with a Hill equation gave values of $K_{0.5}$ and N of 9.6 μM and 0.7 (Fig. 4 *A*, *solid symbols*). The main difference compared with glass tubes was that fura-2 fluorescence within the cells never dropped below 20% of the initial fluorescence even in the presence of millimolar Mn^{2+} suggesting that part of the dye has been trapped in cell compartments out of reach of Mn^{2+}. Using the in vivo relationship and the measured membrane surface area in each cell tested (see Methods), the quenching rates measured at different membrane potentials were converted into membrane current densities (Fig. 4 *C*). At −80 mV the calculated average current density was 2.2 ± 0.6 mA/F and the amplitude of the membrane current in

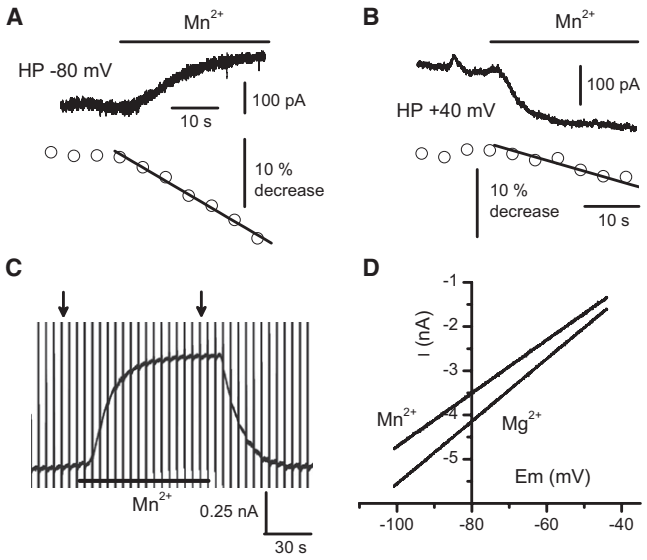

FIGURE 3 Membrane currents evoked by replacement of Mg^{2+} by Mn^{2+}. (*A* and *B*) Simultaneous recordings of membrane currents and fura-2 fluorescence at −80 mV and +40 mV. The slope of the linear fit is 24% and 12%/min at −80 and +40 mV, respectively. (*C*) Continuous recording of membrane current at −80 mV in response to replacement of 10 mM Mg^{2+} by 10 mM Mn^{2+}. The cell was challenged by voltage ramps given from −40 to −100 mV at a rate of 120mV/s every 5 s in the presence of 140 mM external TEA-methanesulfonate plus 9AC and 120 mM internal Cs-aspartate. (*D*) Current-voltage relationships obtained in the fiber illustrated in (*C*) in response to voltage ramps, the lower and upper traces corresponding to the left and right arrows in (*C*), respectively.

the 10 cells tested at −80 mV ranged from 0.8 to 9.8 pA, values that are far below the resolution capacity under voltage-clamp conditions in the whole cell configuration.

Mn^{2+} entry in active muscle

Another series of experiments was carried out to explore whether Mn^{2+} entry could be modified by muscle activity. Trains of AP were evoked at tetanic frequency (50 Hz) under current clamp conditions in cells loaded with fura-2 and the rate of decrease of fluorescence induced by the Mn^{2+} entry was simultaneously monitored (Fig. 5 *A*). The fluorescence intensity was not changed in response to fiber stimulation in the absence of external Mn^{2+} giving evidence that basal resting fluorescence was not altered by intracellular Ca^{2+} changes in fibers excited at 360 nm. Then, during the continuous presence of Mn^{2+}, two consecutive bursts of AP induced a large increase in the influx of Mn^{2+}. The Mn^{2+} influx was on average 29 ± 4 times higher ($n = 18$, $p < 0.001$, paired *t*-test) during a train of AP than under resting conditions.

Previous studies performed on adult skeletal muscle cells have shown that Mn^{2+} entry can be increased by depolarization (13) and by depletion of the SR (10), which possibly occurs during activity. A first set of experiments explored how store depletion could alter Mn^{2+} quenching. As illustrated in Fig. 5 *A*, trains of AP first induced an increase in the influx of Mn^{2+} (Fig. 5 *B*). After returning to resting conditions, addition of the potent inhibitor of the SR Ca^{2+}-ATPase CPA to the external solution did not induce any major change in the rate of Mn^{2+} influx in this cell, although, on average, the drug evoked a slight but significant decrease of 23 ± 8% in the quenching rate ($n = 14$, $p = 0.014$, paired *t*-test). In the continuous presence of CPA, a train of stimulations evoked an elevation of fura-2 fluorescence that likely resulted from the prolonged contracture of the cell that concentrated the dye. Upon repolarization, the resting influx of Mn^{2+} was increased and on average it was 1.8 ± 0.4 times ($n = 11$, $p = 0.045$, paired *t*-test) that measured before stimulation. Also, measurement of the voltage drop resulting from hyperpolarizing pulses of 2 nA amplitude indicated that the input resistance of the cell was not significantly changed in the presence of CPA after (5.4 ± 0.5 MΩ) compared with before stimulation (5.5 ± 0.5 MΩ) ($n = 11$, $p = 0.11$, paired *t*-test). The resting membrane potential was also not significantly changed (−83.1 ± 0.38 mV before and −82.6 ± 0.64 after stimulation, $n = 11$, $p = 0.29$, paired *t*-test). SR depletion was certainly only partial under our experimental conditions because fibers still contracted in the presence of CPA although they contracted weaker and failed to relax after stimulation. However, all our attempts to induce more severe depletion to the point of complete fiber exhaustion systematically led to an irreversible depolarization of the fiber associated with a large fall in the input resistance and a profound and irreversible increase in the influx of Mn^{2+} that saturated the dye. Fig. 5 *C* illustrates such behavior in a particular fiber that displayed irreversible damages as soon as stimulation was delivered in the presence of CPA. This result emphasizes that voltage control is essential to monitor cell integrity during quenching experiments.

Voltage dependence and Cd^{2+} inhibition of Mn^{2+} influx in active muscle

Another set of experiments was carried out to investigate how depolarization by itself initiates Mn^{2+} influx. Mn^{2+} influx together with membrane currents were measured in fibers stimulated by voltage pulses of increasing amplitudes in the presence of 3 mM Mn^{2+}. In these experiments, the possible contribution of a store-operated Mn^{2+} influx should be largely minimized since depolarization has been demonstrated to strongly inhibit store-operated Mn^{2+} influx (10). Fig. 6 shows that 100-ms duration depolarizing pulses given to −50, −30, and −10 mV did not change the rate of Mn^{2+} influx. A pulse to +10 mV induced an inward Mn^{2+} current which reached −1.9 nA, associated with a 9.2% decrease in fluorescence. A subsequent pulse to +30 mV gave rise to an inward Mn^{2+} current that activated faster and reached −2.1 nA, accompanied by a 14.6% drop in fluorescence. Finally, a last pulse to +50 mV induced an outward membrane current associated with a 12% decrease in fluorescence. Inward currents evoked by membrane depolarization were completely blocked by the addition of 0.5 mM Cd^{2+} in

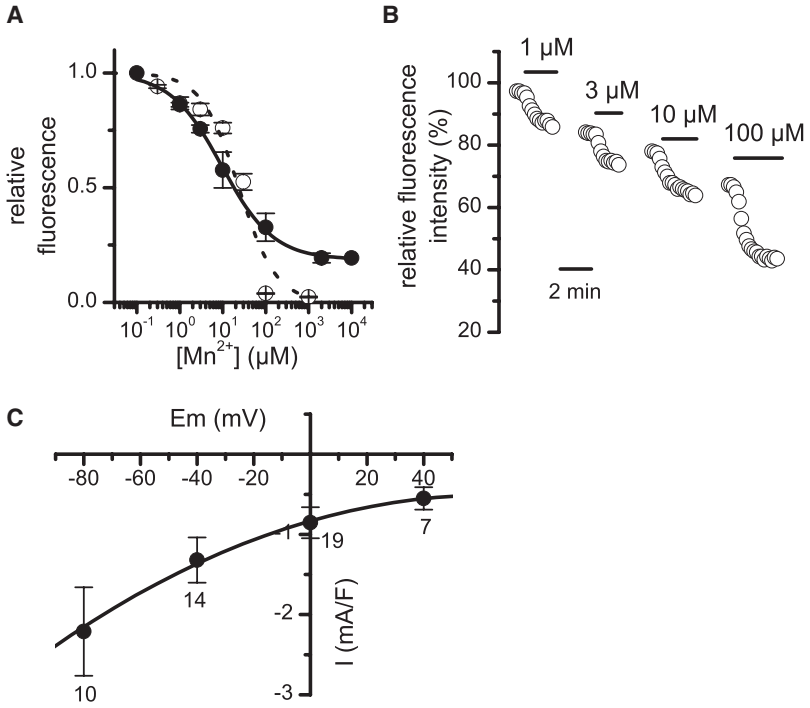

FIGURE 4 Estimation of the sarcolemmal Mn^{2+} current on the basis of the measurement of the changes in fura-2 fluorescence induced by Mn^{2+} entry. (*A*) Relationships between the relative fluorescence of fura-2 and the concentration of Mn^{2+} in glass tubes (*open symbols*, $n = 9$), and the concentration of Mn^{2+} in the external solution bathing muscle fibers in the presence of ionomycin (*solid symbols*, $n = 4$). Curves were fitted using a Hill equation (see text for details). (*B*) Quenching of fura-2 fluorescence obtained in a fiber exposed to the indicated concentrations of Mn^{2+} in the presence of ionomycin. (*C*) Relationship between the estimated resting Mn^{2+} current and membrane voltage. The curve was drawn by eye.

the external solution (Fig. 7 *A*). Taken together, these data likely indicated that the recorded Mn^{2+} current flowed through L-type Ca^{2+} channels, which are known to be permeable to Mn^{2+} in skeletal muscle (18). Fig. 7 *A* presents the voltage-current relationship of the Mn^{2+} current and Fig. 7 *B* superimposes the relationship between the magnitude of the fluorescence decrease induced by Mn^{2+} entry and voltage and the voltage dependence of the relative conductance of the Mn^{2+} current. It can be observed that the voltage-activated Mn^{2+} current and the Mn^{2+} influx were maximal around +30 mV. Fitting Boltzmann equations to these two relationships indicated that $V_{0.5}$ was 24 mV more negative for the Mn^{2+} influx than for the voltage-activated current and that the voltage dependence of the Mn^{2+} influx was steeper than the one of the normalized conductance (k was 4.7 compared with 8.6) (Fig. 7 *B*). Differences suggest that at least two processes displaying dissimilar voltage dependences may contribute to the influx of Mn^{2+}: the L-type current and a parallel voltage-activated Mn^{2+} entry. To determine to what extent each of these two processes contributed to the influx of divalent cations during physiological activation of muscle cells, the effects of a blockade of the L-type current by Cd^{2+} were tested on the influx of Mn^{2+} induced by trains of AP. As illustrated in Fig. 7 *C*, the mean drop in fluorescence induced by the train of excitation in the presence of Cd^{2+} (0.5 mM) was not significantly different from the one induced in its absence ($n = 9$, $p = 0.39$, paired t-test). This result can be interpreted in two ways. Either the L-type current is not activated during trains of AP, or the L-type current is activated, but the influx of Mn^{2+} that this current generates does not contribute significantly to the quenching of fluorescence induced by depolarization. To discriminate between these two possibilities, we tested the effects of Cd^{2+} on the Mn^{2+} influx induced by depolarization. Fig. 7 *D* shows that the decrease in fluorescence in response to a depolarization to +30 mV that evoked an L-type current of maximal amplitude was greatly reduced in the presence of Cd^{2+}. Fig. 7 *B* presents the mean changes in fluorescence induced by different depolarization pulses in the presence of Cd^{2+}. On average, the Mn^{2+} influx was significantly reduced by 72%, 76%, and 82% for depolarization steps to +10, +30, and +50 mV in the presence of Cd^{2+} but was not significantly affected for pulses to −10 mV ($p = 0.46$, unpaired t-test) (Fig. 7 *B*). Fig. 7 *B* also indicated that a substantial Mn^{2+} influx occurred through L-type channels at the reversal potential of the L-type current; however this reversal potential value was likely shifted toward negative voltages by contaminating outward currents so that there still was a driving force for Mn^{2+} influx at +50 mV. Fitting a Boltzmann equation to the relationship between mean changes of fluorescence and membrane potential in the presence of Cd^{2+} gave value for $V_{0.5}$ and k of −8 mV and 4 mV.

DISCUSSION

Properties of divalent cation influx at rest and associated membrane current

In the first part of this study, the combination of the Mn^{2+}-quenching method with a voltage-clamp technique, together with calibration of the fura-2 response to Mn^{2+}, allowed us to thoroughly characterize the influx of divalent cations at rest in isolated adult skeletal muscle fibers. At a holding

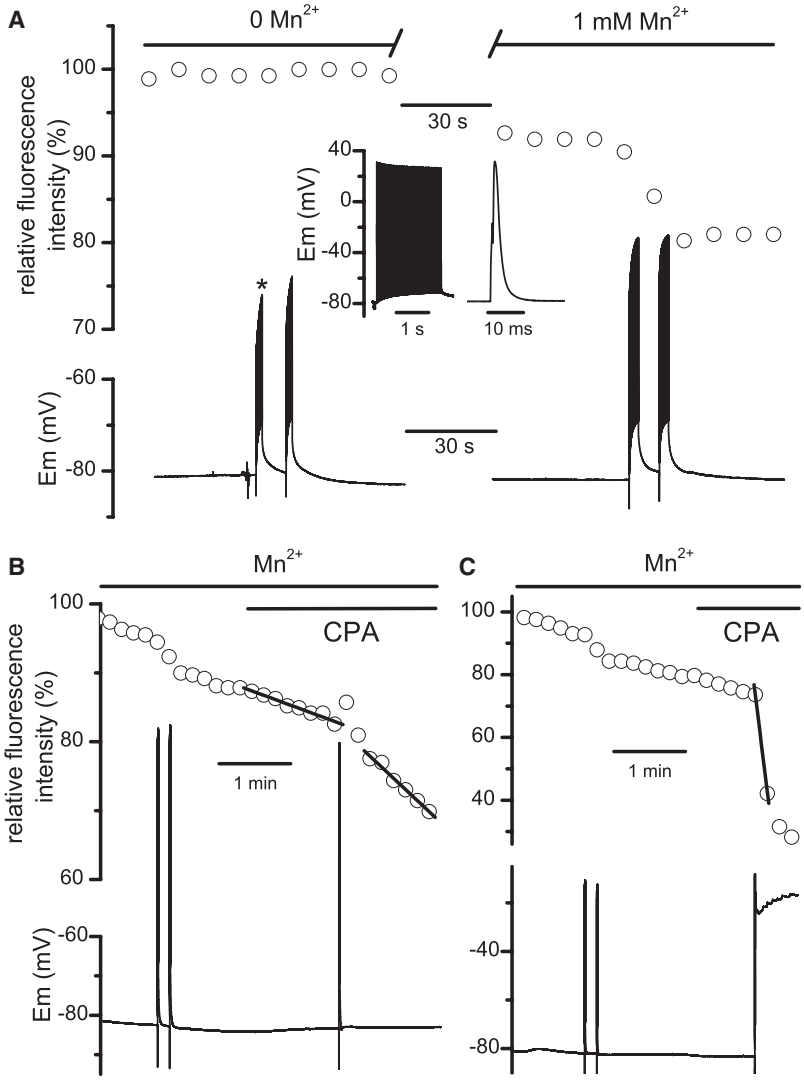

FIGURE 5 Effects of trains of AP and CPA on Mn^{2+} influx under current clamp conditions. (*A*) Simultaneous recordings of fura-2 fluorescence (*open symbols*) and membrane potential (*lower trace*) in a fiber stimulated by positive suprathreshold current pulses of 0.5-ms duration delivered at 50 Hz. The duration of the trains was 2 s in the left panel and 3 s in the right panel. Each burst of stimulation was preceded by a negative current pulse of 2 nA amplitude to measure the fiber input resistance (downward deflections of the voltage trace). The inset shows the first train of AP (*star*, *left trace*) and the first AP of this train (*right trace*) on an expanded scale. The recordings presented in the right panel were obtained in the same fiber 4 min after the ones presented in the left panel. The external Tyrode solution contained 2 mM $CaCl_2$ and 2 mM $MgCl_2$ in which 1 mM Mn^{2+} was added. (*B*) In the continuous presence of a Tyrode solution containing 3 mM Mn^{2+}, the fiber was stimulated by bursts of AP of 500 ms duration delivered at 50 Hz in the absence and in the presence of CPA. Fluorescence records were fitted with a linear regression in the presence of CPA with slopes of 4%/min before and of 10%/min after stimulation. (*C*) In this particular fiber, a single burst of AP given in the presence of CPA led to a brutal drop of fluorescence (the slope of the linear fit is 190%/min) and an irreversible depolarization of the fiber. Note that membrane potential in lower traces was acquired at 200 Hz so that peak values of AP could not be resolved.

potential of −80 mV and in the presence of 500 μM external Mn^{2+}, the rate of Mn^{2+} influx was found to be 4.5% on average, a value close to the values reported in other studies using the same external [Mn^{2+}] on adult mouse muscle fibers at rest (5,9,10,19). The rate of quenching was found to depend on the Mn^{2+} concentration and on the electrical gradient. The voltage dependence of the rate of quenching indicated that the influx of Mn^{2+} was slightly favored at negative membrane potentials, a result that explains that hyperpolarizing steps were less effective in increasing the quenching rate when they were applied from depolarized holding potentials. This apparent inward rectification may either result from intrinsic properties of the pathway involved or be due to the fact that a Mn^{2+} equilibrium potential can never be reached because Mn^{2+} ions are supposed to be unable to move out of the cell. Finally, we observed that the quenching rate was reduced by more than half when Ca^{2+} ions were present at physiological concentrations in the external solution, which indicates that Ca^{2+} competes with Mn^{2+} for permeating the influx pathway.

The combined use of voltage clamp and Mn^{2+}-quenching techniques prompted us to try measuring the inward current that may be associated with Mn^{2+} entry. Mn^{2+} exerted a strong blocking effect on muscle background conductances, which precludes revealing a putative inward current upon replacement of Mg^{2+} by Mn^{2+}. Nevertheless, our in vivo calibration experiments of the fura-2 response to Mn^{2+} predicted that the inward current generated by the influx of Mn^{2+} should have had amplitudes of a few picoamps in the presence of millimolar external [Mn^{2+}], which are clearly undetectable at the macroscopic level. At first sight, these results are hardly reconcilable with data obtained at the single channel level. Openings of spontaneously active Ca^{2+} channels are indeed routinely recorded in cell-attached patches at negative voltages (6) and these channels were found to be permeant to Mn^{2+} (5). However, no correlation was found between subsarcolemmal Ca^{2+} load and activity of these channels, suggesting that they are not involved in resting Ca^{2+} influx (7). For obscure reasons, a parallel pathway that does not produce resolvable current could

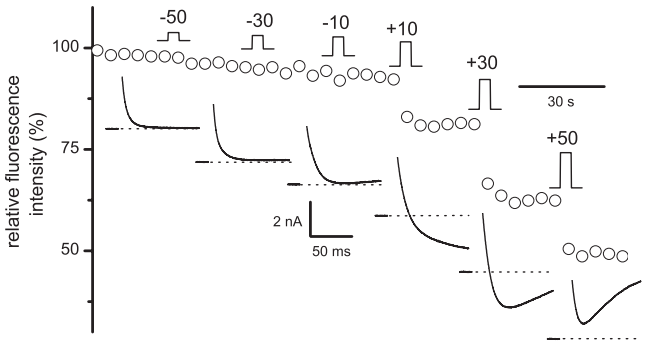

FIGURE 6 Effect of depolarization steps of increasing amplitude on Mn^{2+} influx under voltage-clamp conditions. Fura-2 fluorescence (*open symbols*) and membrane currents (*lower traces*) were measured on the same muscle fiber in the presence of a 140 mM TEA-methanesulfonate Ca^{2+}-free external medium containing 3 mM Mn^{2+}. The cell was held at −80 mV, and voltage steps of 100-ms duration bringing the membrane potential to the indicated values were applied between two fluorescence image captures at the indicated position of the steps. Note that the corresponding currents were positioned under the voltage steps on a different time scale.

thus be more efficient in getting Ca^{2+} in. Yet, the fact that Mn^{2+} entry is driven by the concentration and electrical gradients strongly suggests that Mn^{2+} and Ca^{2+} enter muscle cells through ion channels spontaneously open at rest and necessarily of very low conductance. However, the involvement of electrically silent transport processes directly or indirectly influenced by the concentration and electrical gradients cannot be excluded and deserves further attention. Finally our study demonstrates that, because Mn^{2+} accumulates in the cytosol, the Mn^{2+}-quenching method offers a higher resolution to monitor the entry of divalent cations at rest than the measurement of currents.

Store depletion-activated cation influx

We demonstrated here that a single burst of AP delivered in the presence of CPA significantly increased the resting rate of Mn^{2+} influx. We observed that fibers still contracted in response to stimulation in the presence of CPA, indicating that store depletion was not complete under our experimental conditions. In our hands, attempts to provoke deeper depletion of the SR inevitably led to a huge influx of Mn^{2+} and an irreversible depolarization of the fiber associated with a large decrease in the input resistance, which gave evidence of irreversible damages of the sarcolemma, possibly produced by toxic elevation of the intracellular [Ca^{2+}]. As pointed out

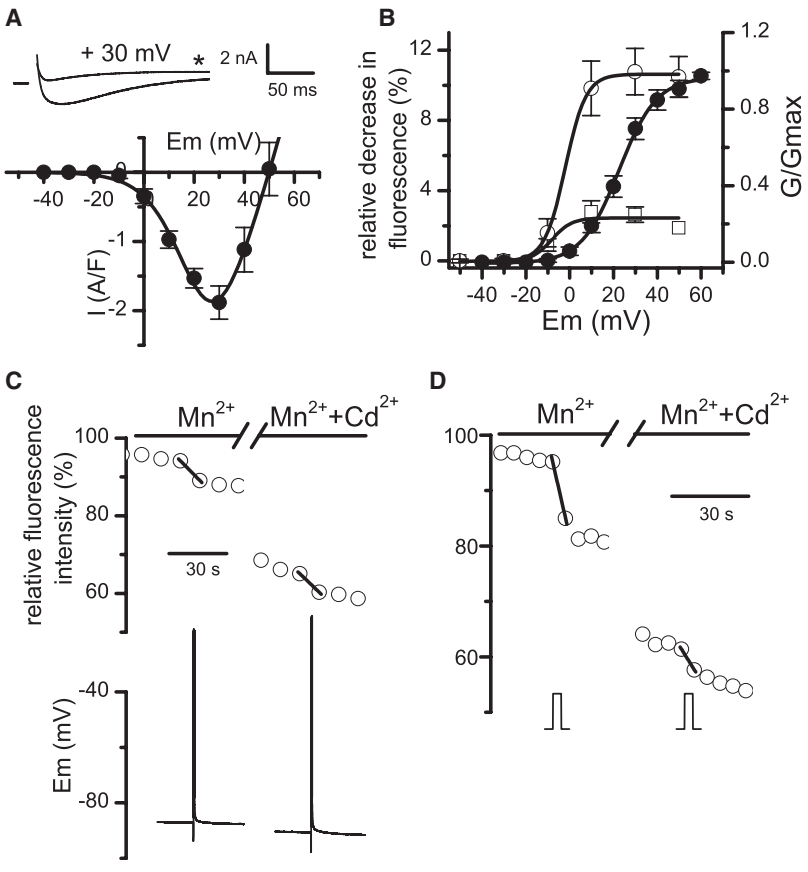

FIGURE 7 Voltage dependence of Mn^{2+} influx and effect of Cd^{2+}. (*A*) The upper traces show the membrane currents recorded in a same fiber in response to a 200-ms depolarization step given to +30mV from a holding potential of −80 mV in the absence and in the presence of 0.5 mM Cd^{2+} (*star*) and the current-voltage relationship of the Mn^{2+} current. The curve was fitted using the equation indicated in Methods with values for G_{max}, V_{rev}, $V_{0.5}$, and k of 127 S/F, +50 mV, +22 mV, and 7.9 mV ($n = 9$). (*B*) Relationships between the mean normalized conductance of the voltage-activated Mn^{2+} current and membrane potential (*solid symbols*), between the mean Mn^{2+} influx, expressed as percentage of decrease of fluorescence, and membrane potential in the absence (*open circles*), and in the presence of 0.5 mM Cd^{2+} (*open squares*). The curves were fitted using a Boltzmann equation with values for $V_{0.5}$ and k of +22 mV and 8.6 mV for the normalized conductance, −1.9 mV and 4.7 mV for the Mn^{2+} influx in the absence of Cd^{2+}, and −8 mV and 4 mV for the Mn^{2+} influx in the presence of Cd^{2+}. The number of cells tested at −10, +10, +30, and +50 mV is 8, 4, 4, and 2 in the absence of Cd^{2+} and 7, 8, 8, and 1 in the presence of Cd^{2+}. (*C*) In the left panel, a single train of AP (*lower trace*) was elicited under current clamp conditions by injection of positive supraliminar current pulses of 0.5-ms duration delivered at 50 Hz in the presence of 3 mM external Mn^{2+}, whereas fura-2 fluorescence was simultaneously recorded (*open symbols*). The same stimulation was applied in the same cell with 0.5 mM Cd^{2+} added in the external medium (right panel). The two consecutive recordings were separated by a 2-min interval. (*D*) In the left panel, the cell was held at −80 mV and a 100-ms depolarizing pulse was given to +30mV as indicated by the step at the bottom in the presence of 3 mM external Mn^{2+}. The same stimulation was applied in the same cell with 0.5 mM Cd^{2+} added in the external medium (right panel). The two consecutive fluorescence recordings were separated by a 1-min interval. The fluorescence data points immediately before and after stimulations were linked by a straight line to make fluorescence drops more visible. The slopes of these lines were 30% and 29%/min in the absence and in the presence of Cd^{2+} in *C*, respectively, and 122% and 45%/min in *D*, respectively.

by Kurebayashi and Ogawa (10), severe Ca^{2+} depletion to the point of complete exhaustion of contraction would certainly never occur in adult skeletal muscle under physiological conditions. Our experiments show that partial depletion does induce Ca^{2+} entry as described by Launikonis and Rios (20) in skinned rat muscle fibers. Confirming our previous data (12), these experiments also demonstrate that the store-operated Ca^{2+} entry was not associated with the development of a measurable current as evidenced by the absence of a significant change in the cell input resistance and membrane potential. This series of experiments also indicates that experiments making use of SR Ca^{2+}-ATPase inhibitors have to be interpreted with caution when they are performed in the absence of voltage control. Background current or membrane potential and input resistance measurement are very reliable indexes of cell integrity that may reveal massive damages of the sarcolemma not related to any store-operated pathway.

Cation influx activated by trains of AP

We found that trains of AP delivered at 50 Hz, which closely correspond to physiological conditions of stimulation, increased Mn^{2+} influx to a much greater degree (29-fold in the presence of 3 mM external Mn^{2+}) compared with store depletion. The control of the membrane potential allowed us to explore the Mn^{2+} influx over a large range of membrane voltages. The following observations led us to conclude that the L-type voltage-activated Ca^{2+} channels and a parallel distinct voltage-activated Mn^{2+} pathway contributed independently to the Mn^{2+} influx in response to depolarization: (i), the voltage dependence of the global Mn^{2+} influx was steeper than the one of the L-type Mn^{2+} current and shifted toward negative potentials; (ii), whereas Cd^{2+} entirely inhibited the L-type Mn^{2+} current, a Mn^{2+} influx still occurred in response to depolarization, with a voltage threshold and voltage dependence that were respectively lower and steeper than those of the L-type current. Our Cd^{2+} experiments also allowed us to estimate the relative contribution of each of these divalent cations entries during muscle activation at different voltages. At -10 mV, the newly identified voltage-activated Mn^{2+} influx pathway may contribute mainly to the global Mn^{2+} influx, whereas for higher depolarizations it may represent between 18% and 28% of the total Mn^{2+} influx. A striking observation was that no net inward current persisted when the L-type current was inhibited by Cd^{2+}. Yet, if this influx represents 24% of the global entry at $+30$ mV, we should have been able to record a net inward current after Cd^{2+} blockade whose amplitude should also represent one quarter of the amplitude of the L-type current. A similar phenomenon identified as excitation-coupled Ca^{2+} entry has been described in myotubes (13) and, interestingly, current recordings on myotubes expressing a mutant isoform of type 1 ryanodine receptor also failed to reveal a current associated with this Mn^{2+} entry although the magnitude of the Ca^{2+} entry produced predicted that a current larger than the L-type current should have developed (21). As postulated for myotubes, our results suggest that a voltage-activated Mn^{2+} influx operates in an electrically silent manner in adult skeletal muscle. One possibility is that this Mn^{2+} influx involves a nonelectrogenic exchanger, which up to now has never been described, but actually merits further consideration.

Physiological significance of activity-induced cation influx

A more striking result was that Cd^{2+} did not affect the Mn^{2+} influx induced by train of AP. Apart from the fact that this result confirms that a voltage-activated Mn^{2+} influx insensitive to Cd^{2+} does operate in adult skeletal muscle in parallel with the L-type current, these data also suggest that the L-type current does not contribute to the influx of divalent cations during physiological excitation. However, this last result must be taken with caution because the voltage dependence of the Mn^{2+} current through L-type channels was shifted by 23 mV toward positive membrane potentials ($V_{0.5} = +22$ mV) compared with the voltage dependence of the Ca^{2+} current in the presence of 2.5 mM external Ca^{2+} ($V_{0.5} = -0.7$ mV in 22). The membrane potential reached in response to trains of AP could thus be far above the peak value of the L-type Ca^{2+} current but lower than the one of the Mn^{2+} current so that the contribution of the L-type current may be minimized when Mn^{2+} ions are flowing through the channels. Whatever the pathway involved, the physiological role of the Ca^{2+} influx during excitation remains largely elusive in skeletal muscle. A current hypothesis suggests that the Ca^{2+} entry induced by depolarization or by SR depletion may contribute to refill internal Ca^{2+} stores, especially under fatigue conditions. However, it was shown that the recovery of the releasable pool after fatigue occurred in the absence of extracellular Ca^{2+} (23), and growing evidence indicates that Ca^{2+} is not extruded from the cells during fatigue but may remain as a nonreleasable pool possibly bound to phosphate within the SR (24). Within this context, we believe that the nature and the physiological role of the Ca^{2+} pathways involved during excitation still remain open questions in adult skeletal muscle and call for further attention.

The authors are grateful to J-L. Barrat, M. Jospin, and V. Jacquemond for helpful comments on the manuscript.

This work was supported by the Université Lyon 1, the Centre National de la Recherche Scientifique, the Association Française contre les Myopathies, and the Agence Nationale de la Recherche Maladies Rares.

REFERENCES

1. Clausen, T., A. B. Dahl-Hansen, and J. Elbrink. 1979. The effect of hyperosmolarity and insulin on resting tension and calcium fluxes in rat soleus muscle. *J. Physiol.* 292:505–526.

2. Gailly, P. 2002. New aspects of calcium signaling in skeletal muscle cells: implications in Duchenne muscular dystrophy. *Biochim. Biophys. Acta*. 1600:38–44.

3. Haws, C. M., and J. B. Lansman. 1991. Developmental regulation of mechanosensitive calcium channels in skeletal muscle from normal and *mdx* mice. *Proc. Biol. Sci.* 245:173–177.

4. Hopf, F. W., P. R. Turner, W. F. Denetclaw, Jr., P. Reddy, and R. A. Steinhardt. 1996. A critical evaluation of resting intracellular free calcium regulation in dystrophic *mdx* muscle. *Am. J. Physiol.* 271:C1325–C1339.

5. De Backer, F., C. Vandebrouck, P. Gailly, and J. M. Gillis. 2002. Long-term study of Ca^{2+} homeostasis and of survival in collagenase-isolated muscle fibres from normal and *mdx* mice. *J. Physiol.* 542:855–865.

6. Allard, B. 2006. Sarcolemmal ion channels in dystrophin-deficient skeletal muscle fibres. *J. Muscle Res. Cell Motil.* 27:367–373.

7. Mallouk, N., and B. Allard. 2002. Ca^{2+} influx and opening of Ca^{2+}-activated K^+ channels in muscle fibers from control and *mdx* mice. *Biophys. J.* 82:3012–3021.

8. Merritt, J. E., R. Jacob, and T. J. Hallam. 1989. Use of manganese to discriminate between calcium influx and mobilization from internal stores in stimulated human neutrophils. *J. Biol. Chem.* 264:1522–1527.

9. Tutdibi, O., H. Brinkmeier, R. Rüdel, and K. J. Föhr. 1999. Increased calcium entry into dystrophin-deficient muscle fibres of MDX and ADR-MDX mice is reduced by ion channel blockers. *J. Physiol.* 515:859–868.

10. Kurebayashi, N., and Y. Ogawa. 2001. Depletion of Ca^{2+} in the sarcoplasmic reticulum stimulates Ca^{2+} entry into mouse skeletal muscle fibres. *J. Physiol.* 533:185–199.

11. Collet, C., and J. Ma. 2004. Calcium-dependent facilitation and graded deactivation of store-operated calcium entry in fetal skeletal muscle. *Biophys. J.* 87:268–275.

12. Allard, B., H. Couchoux, S. Pouvreau, and V. Jacquemond. 2006. Sarcoplasmic reticulum Ca^{2+} release and depletion fail to affect sarcolemmal ion channel activity in mouse skeletal muscle. *J. Physiol.* 575:69–81.

13. Cherednichenko, G., A. M. Hurne, J. D. Fessenden, E. H. Lee, P. D. Allen, et al. 2004. Conformational activation of Ca^{2+} entry by depolarization of skeletal myotubes. *Proc. Natl. Acad. Sci. USA*. 101: 15793–15798.

14. Cherednichenko, G., C. W. Ward, W. Feng, E. Cabrales, L. Michaelson, et al. 2008. Enhanced excitation-coupled calcium entry in myotubes expressing malignant hyperthermia mutation R163C is attenuated by dantrolene. *Mol. Pharmacol.* 73:1203–1212.

15. Jacquemond, V., and B. Allard. 1998. Activation of Ca^{2+}-activated K^+ channels by an increase in intracellular Ca^{2+} induced by depolarization of mouse skeletal muscle fibres. *J. Physiol.* 509:93–102.

16. Weiss, N., H. Couchoux, C. Legrand, C. Berthier, B. Allard, et al. 2008. Expression of the muscular dystrophy-associated caveolin-3^{P104L} mutant in adult mouse skeletal muscle specifically alters the Ca^{2+} channel function of the dihydropyridine receptor. *Pflugers Arch.* 457:361–375.

17. Jacquemond, V. 1997. Indo-1 fluorescence signals elicited by membrane depolarization in enzymatically isolated mouse skeletal muscle fibers. *Biophys. J.* 73:920–928.

18. Almers, W., and P. T. Palade. 1981. Slow calcium and potassium currents across frog muscle membrane: measurements with a vaseline-gap technique. *J. Physiol.* 312:159–176.

19. Fraysse, B., J. F. Desaphy, S. Pierno, A. De Luca, A. Liantonio, et al. 2003. Decrease in resting calcium and calcium entry associated with slow-to-fast transition in unloaded rat soleus muscle. *FASEB J.* 17:1916–1918.

20. Launikonis, B. S., and E. Ríos. 2007. Store-operated Ca^{2+} entry during intracellular Ca^{2+} release in mammalian skeletal muscle. *J. Physiol.* 583:81–97.

21. Hurne, A. M., J. J. O'Brien, D. Wingrove, G. Cherednichenko, P. D. Allen, et al. 2005. Ryanodine receptor type 1 (RyR1) mutations C4958S and C4961S reveal excitation-coupled calcium entry (ECCE) is independent of sarcoplasmic reticulum store depletion. *J. Biol. Chem.* 280:36994–37004.

22. Collet, C., L. Csernoch, and V. Jacquemond. 2003. Intramembrane charge movement and L-type calcium current in skeletal muscle fibers isolated from control and *mdx* mice. *Biophys. J.* 84:251–265.

23. Kabbara, A. A., and D. G. Allen. 1999. The role of calcium stores in fatigue of isolated single muscle fibres from the cane toad. *J. Physiol.* 519:169–176.

24. Allen, D. G., G. D. Lamb, and H. Westerblad. 2008. Skeletal muscle fatigue: cellular mechanisms. *Physiol. Rev.* 88:287–332.